scientific reports

Check for updates

OPEN

# Effect of defective H2B ubiquitination on the malignancy and repair of DNA double breaks and its significance in lung adenocarcinoma

Zhiyuan An[1,2,9], Ningning Yao[3,9], Wenzhong Su[4,9], Weiyang Zhang[2], Junting Yang[5], Qinping Guo[6], Congqiao Zhang[2], Pan Tian[2], Neng Wan[2], Congcong Wu[2], Xiang Huang[7], Guohua Song[5]✉, Junting Jia[8]✉ & Laifeng Ren[2]✉

**Lung cancer is the leading cause of cancer-related mortality, with a notably low five-year survival rate due to the limited availability of effective treatments. Monoubiquitination of histone H2B at lysine 120(uH2B) exerts a tumor-suppressive effect in cancer through multiple mechanisms, including the regulation of transcriptional activity and DNA damage response. Ring Finger Protein 20 (RNF20), a key E3 ubiquitin ligase, plays a central role in this process. However, the role of RNF20 in lung adenocarcinoma (LUAD) progression is unknown. In this study, the functional characterization of the role and molecular mechanism of LUAD were examined using a series of biological and cellular approaches in vitro and in vivo. Our work shows the expression of uH2B is significantly reduced in LUAD patients and is correlated with prognosis. Similarly, RNF20 expression is also markedly decreased in LUAD. Knockdown of RNF20 promoted the proliferation and migration of A549 cells while simultaneously decreasing uH2B expression. Additionally, RNF20 knockdown impaired the DNA damage repair capacity of LUAD cells. RNF20-silenced A549 cells exhibited heightened sensitivity to both the Cisplatin and PARP inhibitor Olaparib. These findings provide an important foundation for further understanding the molecular mechanisms of lung adenocarcinoma and developing new treatment strategies.**

**Keywords** uH2B, RNF20, Lung adenocarcinoma, DNA damage repair, Biomarkers

Lung cancer is one of the most common and deadliest malignant tumors worldwide, with LUAD being the most common subtype[1]. Despite advances in treatment methods in recent years, the five-year survival rate for lung cancer patients remains low, primarily due to low early detection rates and a lack of effective targeted

[1]Central Laboratory, Cancer Hospital Affiliated to Shanxi Medical University/Shanxi Province Cancer Hospital, Shanxi Hospital Affiliated to Cancer Hospital/Chinese Academy of Medical Sciences, Taiyuan 030001, Shanxi, China. [2]Department of Basic Medical Sciences , Shanxi Medical University, Taiyuan 030001, Shanxi, China. [3]Department of Radiotherapy, Shanxi Province Cancer Hospital/Shanxi Hospital Affiliated to Cancer Hospital, Chinese Academy of Medical Sciences/Cancer Hospital Affiliated to Shanxi Medical University, Taiyuan 030001, Shanxi, China. [4]Department of Respiratory, Shanxi Province Cancer Hospital/Shanxi Hospital Affiliated to Cancer Hospital, Chinese Academy of Medical Sciences/Cancer Hospital Affiliated to Shanxi Medical University, Taiyuan 030001, Shanxi, China. [5]Laboratory Animal Center, Shanxi Key Laboratory of Experimental Animal Science and Human Disease Animal Model, Shanxi Medical University, Road Xinjian 56, Taiyuan 030001, Shanxi, China. [6]Department of General Surgery, Tongji Shanxi Hospital, Shanxi Bethune Hospital, Shanxi Academy of Medical Sciences, Third Hospital of Shanxi Medical University, Taiyuan 030001, Shanxi, China. [7]Center of Reproductive Medicine, Shanxi Women and Children Health Hospital, Taiyuan 030001, Shanxi, China. [8]Department of Pharmacy, Shanxi Province Cancer Hospital/Shanxi Hospital Affiliated to Cancer Hospital, Chinese Academy of Medical Sciences/Cancer Hospital Affiliated to Shanxi Medical University, Taiyuan 030001, Shanxi, China. [9]Zhiyuan An, Ningning Yao and Wenzhong Su contributed equally to this work. ✉email: ykdsgh@163.com; jiajunting106@163.com; rlaifeng@163.com

therapies[2]. Therefore, gaining a deeper understanding of the molecular mechanisms of LUAD and identifying new biomarkers and therapeutic targets are of great significance in improving the survival rate of patients.

Histone modifications, such as monoubiquitination of histone H2B at lysine 120, play a critical role in regulating chromatin structure and transcriptional activity[3]. As a dynamic marker associated with activity of transcription and DNA damage repair, uH2B serves as an essential modulator of genomic stability[4,5]. The enzymatic machinery responsible for uH2B, particularly the RNF20/RNF40 E3 ubiquitin ligase complex, has emerged as a key regulator of this process[6]. RNF20 is a central mediator in this ubiquitin ligase complex, facilitating the addition of ubiquitin to H2B. Additionally, the RNF20/RNF40 complex, in cooperation with specific E2 enzymes, catalyzes the ubiquitination of H2B, thereby enhancing transcriptional activity[7]. This interplay highlights RNF20 as a crucial factor linked to the functional regulation of uH2B, making it an important subject for exploring chromatin modifications and their implications in cancer biology.

RNF20 plays pivotal roles in maintaining genomic stability through its involvement in DNA damage response, chromatin remodeling, and transcriptional regulation via histone H2B lysine 120 ubiquitination[8]. Emerging evidence links RNF20 dysregulation to tumorigenesis across multiple cancers, including lung adenocarcinoma[9]. In LUAD, RNF20-mediated UH2B governs chromatin dynamics to regulate gene expression programs critical for cellular homeostasis[3]while also facilitating DNA damage recognition and repair through recruitment of homologous recombination (HR) machinery[10]. Interestingly, Tarcic et al. further revealed significant subtype heterogeneity in RNF20/UH2B function in breast cancer studies[11]indicating that its tumor regulatory role may be highly dependent on specific tumor microenvironments and molecular subtypes.

Although previous studies have shown the involvement of H2B ubiquitination in various tumors, its specific role and mechanism in lung adenocarcinoma are still unclear. In this study, we investigated the molecular mechanism by which RNF20 regulates uH2B protein abundance. We demonstrated that RNF20 interacts and regulate uH2B protein stabilization In LUAD cells. We further demonstrated that knockdown of RNF20 in LUAD cells suppressed cell proliferation and migration ability. Additionally, loss of RNF20 promoted tumor growth in a mouse xenograft model. Our study demonstrated that diminished RNF20 expression is associated with HRR defects, including enhanced sensitivity to radiation, delayed recruitment of key HRR components and reduced HRR efficiency. Thus, preclinical studies in RNF20-deficient models suggest that combining cisplatin with PARP inhibitors such as olaparib may represent a promising therapeutic strategy for LUAD patients, particularly those harboring homologous recombination repair deficiencies.

## Results

### uH2B is markedly reduced expression in LUAD and correlated with poor prognosis

To investigate the significance of uH2B expression in LUAD, we performed immunohistochemical (IHC) analysis on 162 LUAD tissues and their matched noncancerous lung tissues. uH2B nuclear immunostaining was negative or weakly positive (score < 6) in 92.6% of LUAD tissues (150 of 162 cases). In contrast, normal lung tissues displayed robust nuclear uH2B signals (score ≥ 6) in 96.5% of cases (55/57), starkly contrasting with the weak or absent staining in LUAD samples. ($P < 0.0001$) (Fig. 1a and b). We further evaluated the relationship between uH2B and survival in LUAD patients. The Kaplan-Meier survival analysis revealed that while uH2B gene mutations in LUAD patients are not significantly correlated with overall survival (OS) or progression-free survival (PFS), patients with low uH2B expression exhibit markedly poorer prognoses for both OS and PFS. (Figure 1c and d). Furthermore, uH2B expression was associated with the clinical stage and recurrence of LUAD, with lower uH2B expression levels in the patients with later-stage disease ($\chi^2 = 5.031$, $P = 0.025$, Table 1) and in the patient experienced recurrence ($\chi^2 = 5.771$, $P = 0.016$, Table 1). However, uH2B protein expression was not associated with patient gender, age, smoking history, p-TNM staging, or EGFR mutations ($P > 0.05$, Table 1). Cox univariate regression analysis showed that gender, smoking history, T stage, N stage, clinical stage, recurrence status, and high expression of uH2B protein were all significant risk factors for the prognosis of lung adenocarcinoma ($P < 0.05$). Furthermore, Cox multivariate regression analysis revealed that T stage, N stage, and recurrence status were independent prognostic risk factors for lung adenocarcinoma ($P < 0.05$, Table 2).

### Abnormal expression of RNF20 in LUAD and LUSC

Using the Sanger Box 3.0 tool to analyze TCGA data, we identified significant downregulation of RNF20 mRNA expression in tumor tissues compared to normal tissues across eight cancer types, including lung adenocarcinoma (LUAD) ($P < 0.0001$). While, lung squamous cell carcinoma (LUSC) exhibited only a modest reduction in RNF20 expression (Fig. 2a). This differential downregulation was further validated using the UALCAN platform, confirming a pronounced decrease in RNF20 levels in LUAD ($P = 0.014$, Fig. 2b) and a milder reduction in LUSC ($P = 0.002$, Fig. 2f). Notably, RNF20 expression was significantly associated with TP53 mutation status in both subtypes: LUAD and LUSC samples harboring TP53 mutations displayed markedly lower RNF20 levels compared to TP53 wild-type counterparts (Fig. 2c, g). Survival analyses via GEPIA revealed no significant differences in RNF20 expression between these two lung cancer subtypes for both overall survival (OS) and disease-free survival (DFS) ($P > 0.05$, Fig. 2d, e, h and i).

### Downregulation of RNF20/UH2B signaling inhibits proliferation and migration in the lung epithelial cell line A549

To investigate the role of RNF20 in lung adenocarcinoma, A549 cells were transfected with lentiviruses carrying RNF20-specific shRNA (RNF20 shRNA) or an empty vector as a negative control (Control shRNA). Transfection efficiency was confirmed using fluorescence microscopy, where GFP expression was observed in over 80% of transfected cells, indicating high transduction efficiency (Fig. 3a). The knockdown effect of RNF20 protein was verified by Western blot (Fig. 3b). Furthermore, the modulation of UH2B protein levels in A549 cells was analyzed. Compared to the Control shRNA group, knockdown of RNF20 resulted in a moderate

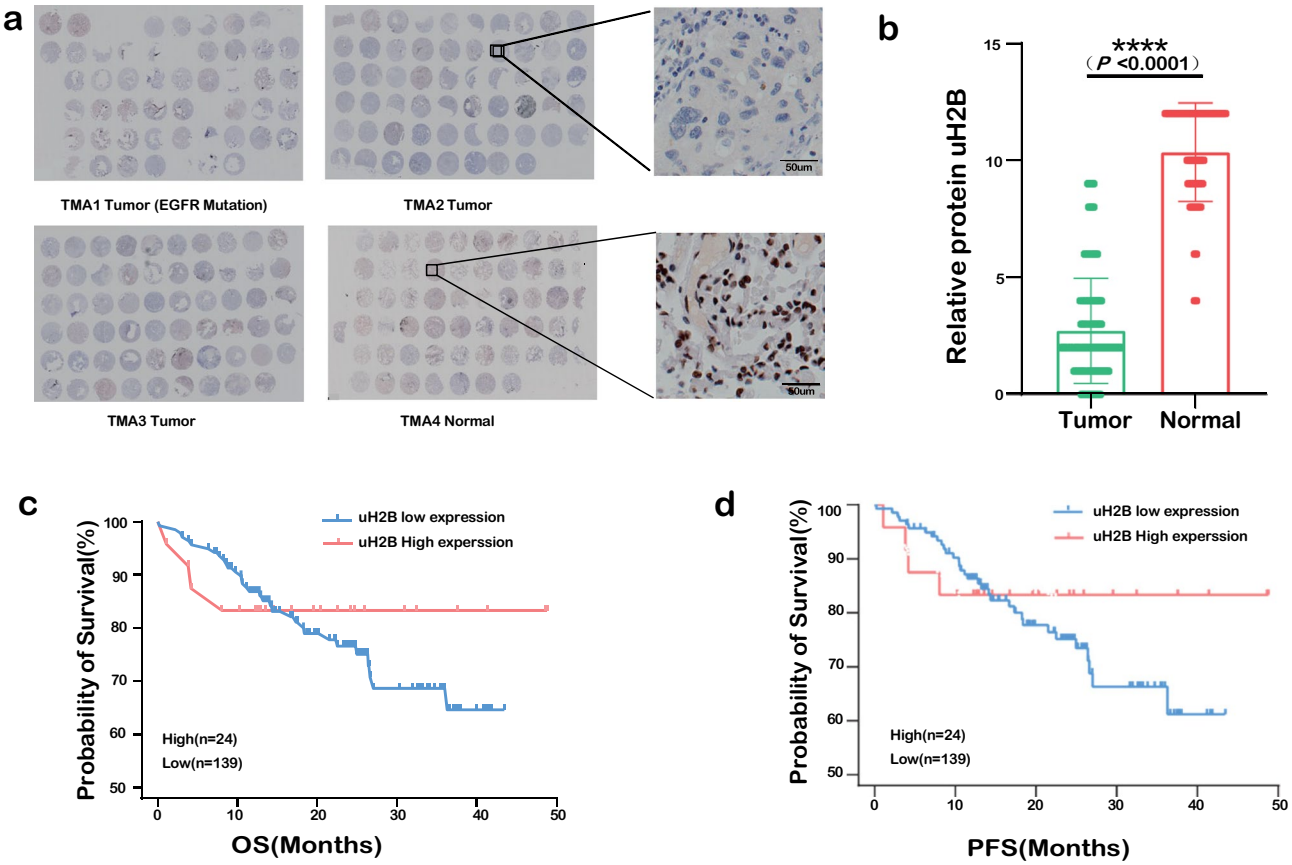


**Fig. 1**. Protein Expression of uH2B in LUAD and prognosis. (a) IHC staining of tissue microarray (TMA) sections showing uH2B expression in LUAD tissues and adjacent normal tissues (magnification: 0.4×). High-power magnification (40×) highlights two tissue spots. Scale bar: 50 μm. (b) Quantitative analysis shows that uH2B expression is significantly lower in LUAD tissues compared to adjacent normal tissues. (c) Kaplan-Meier survival analysis comparing overall survival (OS) between patients with high and low uH2B expression. (d) Kaplan-Meier survival analysis comparing progression-free survival (PFS) between patients with high and low uH2B expression. (****$P$ <0.0001)

decrease in UH2B expression (Fig. 3b), demonstrating that RNF20 shRNA effectively downregulates RNF20 and UH2B in A549 cells. Moreover, the CCK-8 assay demonstrated significantly increased cell proliferation in the RNF20-deficient group compared to controls at 24 h, 48 h, and 72 h ($P$=0.002), while Western blot analysis confirmed stable knockdown efficiency with no time-dependent differences in RNF20 protein levels post-silencing (Fig. 3c). The cells were observed under an inverted microscope 24 h post-scratch, revealing that all groups displayed some migration into the scratch area. At 24 h, cell migration was significantly greater in the RNF20 shRNA group compared to the control group, and by 36 h, the scratch area was almost fully covered by the RNF20-deficient cells (Fig. 3d). These findings suggest that RNF20 knockdown significantly enhances the migratory capability of lung adenocarcinoma cells.

## Knockdown of RNF20 enhances in vivo growth of lung adenocarcinoma

To assess whether RNF20 knockdown enhances the in vivo tumorigenicity of A549 cells, we transplanted RNF20 shRNA-A549 and Control shRNA-A549 cells into the buccal mucosa of immunodeficient Chinese hamsters. LUAD tumors were successfully developed within three days post-transplantation. Immunostaining of the tumors showed strong and uniform expression of luminal markers, including MAGE-A and CK8, indicating successful tumor formation (Fig. 4a). We further compared the tumorigenic properties of RNF20 shRNA-A549 and Control shRNA-A549 cells. Hematoxylin and eosin (H&E) staining of the tumors revealed irregular nuclear morphology, increased chromatin, and enhanced nuclear division in the RNF20 knockdown tumors, indicative of a more undifferentiated and aggressive phenotype (Fig. 4b). To quantify tumor growth, we trypsinized both RNF20 shRNA-A549 and Control shRNA-A549 cells, collected $2\times10^6$ viable cells in 0.1 ml PBS, and injected them into the buccal mucosa of Chinese hamsters. LUAD tumors were successfully formed within three days. The RNF20 shRNA group exhibited significantly larger tumor volumes compared to the control group, suggesting that RNF20 knockdown promotes accelerated tumor growth in vivo (Fig. 4c and d).

| Clinicopathological variables | *n* | uH2B | | $\chi^2$ | *P* |
|---|---|---|---|---|---|
| | | Low expression (*n* = 139) | High expression (*n* = 24) | | |
| Gender | | | | | |
| Male | 92 | 81 | 11 | 1.288 | 0.256 |
| Female | 71 | 58 | 13 | | |
| Age(years) | | | | | |
| < 60 | 68 | 57 | 11 | 0.196 | 0.658 |
| ≥ 60 | 95 | 82 | 13 | | |
| Smoking | | | | | |
| YES | 78 | 69 | 9 | 1.209 | 0.272 |
| NO | 85 | 70 | 15 | | |
| T staging | | | | | |
| T1 + T2 | 104 | 85 | 19 | 2.287 | 0.09 |
| T3 + T4 | 59 | 54 | 5 | | |
| N staging | | | | | |
| NO + N1 | 98 | 81 | 17 | 1.34 | 0.246 |
| N2 + N3 | 65 | 58 | 7 | | |
| M staging | | | | | |
| MO | 155 | 132 | 23 | 0.033 | 0.856 |
| M1 | 8 | 7 | 1 | | |
| Clinical staging | | | | | |
| I + II | 81 | 64 | 17 | 5.031 | 0.025 * |
| III + IV | 82 | 75 | 7 | | |
| Recurrence | | | | | |
| YES | 38 | 37 | 1 | 5.771 | 0.016* |
| NO | 125 | 102 | 23 | | |
| EGFR | | | | | |
| Fusion | 46 | 40 | 6 | 0.143 | 0.205 |
| Unfused | 64 | 54 | 10 | | |

**Table 1**. Relationship between uH2B expression and clinicopathological parameters in LUAD. uH2B: Monoubiquitination of histone H2B at lysine 120.

## RNF20 knockdown impairs DNA damage repair in lung adenocarcinoma cells

To investigate the effect of RNF20 knockdown on DNA damage repair in A549 cells, we analyzed γH2AX and RAD51 expression in both RNF20 shRNA-A549 and Control shRNA-A549 cells. With γH2AX positivity initially lower in the RNF20 shRNA group at 1 h but significantly higher at 4 h and 24 h post-irradiation compared to the control group (Fig. 5a and c). Additionally, RAD51 foci formation, indicative of homologous recombination repair, was assessed by immunofluorescence. At 0 h post-irradiation, no differences were observed between the two groups; However, at 4 h, RAD51 foci formation was significantly reduced in RNF20 shRNA-A549 cells compared to the control group (Fig. 5b and d). These results collectively show that RNF20 knockdown impairs both DNA damage response and homologous recombination repair in A549 cells, highlighting the critical role of RNF20 in maintaining DNA repair capacity in lung adenocarcinoma.

## RNF20 knockdown sensitizes A549 cells to PARP inhibitors and cisplatin

To investigate the impact of RNF20 knockdown on chemotherapy sensitivity, we assessed cell viability 72 h after treatment with commonly used cancer drugs. RNF20 shRNA-A549 cells were highly sensitive to Cisplatin, with cell viability reduced to one-fifth at a concentration of 2 μM, while Control shRNA-A549 cells exhibited considerable resistance with only slight viability reduction (Fig. 6a). Similarly, RNF20 shRNA-A549 cells displayed significant hypersensitivity to the PARP inhibitor Olaparib, retaining only one-third of cell viability at a concentration of 20 μg/ml compared to untreated controls, whereas Control shRNA-A549 cells showed minimal cell viability loss under the same conditions (Fig. 6b). Additionally, RNF20 shRNA-A549 cells exhibited markedly increased sensitivity when treated with a combination of Olaparib and Cisplatin compared to the control group (Fig. 6c). These findings highlight that RNF20 knockdown significantly enhances the chemosensitivity of A549 cells to both PARP inhibitors and Cisplatin, suggesting a potential therapeutic vulnerability in RNF20-deficient lung adenocarcinoma cells.

| Clinicopathological variables | Cox univariate analysis | | | Coxmultivariate analysis | | |
|---|---|---|---|---|---|---|
| | HR | 95%CI | *P* | HR | 95%CI | *P* |
| Gender (Female VS. Male) | 2.386 | 1.124-5. 065 | 0.024 | | | |
| Age (≥ 60 years VS. < 60 years) | 0.678 | 0.34–1.3 49 | 0.268 | | | |
| Smoking (YES VS. NO) | 0.415 | 0.208-0. 827 | 0.012 | | | |
| T staging (T3 + T4 VS. T1 + T2) | 0.424 | 0.219-0. 821 | 0.011 | 0.394 | 0.19–0.8 14 | 0.012 |
| N staging (N0 + N1 VS. N2 + N3) | 0.482 | 0.25–0.9 26 | 0.029 | 0.356 | 0.13–0.9 78 | 0.045 |
| M staging (M1 VS. M0) | 0.595 | 0.182-1. 941 | 0.389 | | | |
| Clinical staging (I + II VS. III + IV) | 0.447 | 0.227-0. 884 | 0.021 | | | |
| Lymph node metastasis (Yes VS. No) | 1.41 | 0.735-2. 708 | 0.301 | | | |
| Recurrence (YES VS. NO) | 2.348 | 1.224-4. 504 | 0.01 | 2.323 | 1.182-4. 565 | 0.014 |
| EGFR mutation (YES VS. NO) | 0.72 | 0.336-1. 542 | 0.398 | | | |
| KRAS mutation (YES VS. NO) | 1.22 | 0.604-2. 463 | 0.58 | | | |
| uH2B (Low expression VS. High expression) | 0.714 | 0.252-2. 028 | 0.527 | 0.787 | 0.261-2. 368 | 0.669 |

**Table 2**. Univariate and multivariate Cox regression analysis of factors associated with OS in LUAD.

## Discussion

Lung cancer remains one of the deadliest malignancies worldwide, with both incidence and mortality rates consistently high despite significant advances in medical technology[12]. Cisplatin(DDP), a first-line chemotherapeutic agent for LUAD, often induces resistance in malignant cells, contributing to tumor progression and recurrence[10]. In this study, we confirmed the reduced expression of uH2B in LUAD and used a novel Chinese hamster model to show that RNF20 knockout promotes in vivo growth of lung adenocarcinoma. We also demonstrated that defects in homologous recombination repair offer a new strategy for overcoming cisplatin resistance in lung adenocarcinoma.

In the present study, we initially confirmed the markedly reduced expression of uH2B in LUAD tissues compared to adjacent normal tissues ($P < 0.0001$) aligns with prior studies suggesting that uH2B is a hallmark of active transcription and genomic stability[13]. The reduced levels in LUAD may reflect a shift in transcriptional activity or increased chromatin instability within tumor cells, potentially contributing to tumorigenesis[14,15]. The association between low uH2B expression and later-stage disease, as well as recurrence ($P < 0.05$), further suggests that uH2B downregulation could facilitate more aggressive cancer phenotypes. Interestingly, while uH2B expression was not associated with patient gender, age, or EGFR mutation status, its links to clinical stage and recurrence highlight its specificity as a cancer progression marker. These observations warrant further investigation into whether uH2B could serve as a therapeutic target to modulate chromatin function in LUAD.

Our comprehensive pan-lung cancer analysis reveals several important insights regarding RNF20 dysregulation across histological subtypes. The TCGA data demonstrate a striking dichotomy in RNF20 downregulation between LUAD and LUSC, with LUAD showing significantly more pronounced suppression ($P < 0.0001$ vs. $P < 0.05$). This differential expression pattern suggests potential subtype-specific mechanisms of RNF20 regulation, possibly related to their distinct cellular origins and molecular landscapes. Notably, the consistent association between RNF20 downregulation and TP53 mutations across both LUAD and LUSC subtypes underscores the potential biological significance of the p53-RNF20 regulatory axis in lung cancer pathogenesis.

In this study, the findings demonstrate that RNF20 knockdown significantly enhances the proliferative and migratory capacity of A549 cells (Fig. 3c and d), supporting its putative tumor suppressive role in lung adenocarcinoma. The sustained depletion of both RNF20 and its catalytic product uH2B across all time points (Fig. 3b and c) suggests this phenotype arises through disrupted epigenetic control. Specifically, the observed reduction in uH2B, a key histone mark governing transcriptional fidelity and DNA damage response, likely compromises genomic stability while promoting oncogenic transcriptional programs. Consistent with recent studies[4,7]our findings establish the RNF20/uH2B signaling pathway as a critical regulator of tumor progression.

We employed a novel method to establish a lung adenocarcinoma model by injecting tumor cells directly into the oral cheek pouch. Tumors reached their maximum size by the third day, at which point tumor tissues were harvested for analysis. Immunofluorescence staining demonstrated positive results for the lung adenocarcinoma-specific antibody MAGE-A and the tumor marker CK8[16,17]. Hematoxylin and eosin (HE) staining revealed poorly differentiated cancer cells, confirming the successful establishment of the lung adenocarcinoma model. To further investigate, we injected control shRNA-A549 and RNF20 shRNA-A549 cells into the cheek pouches.

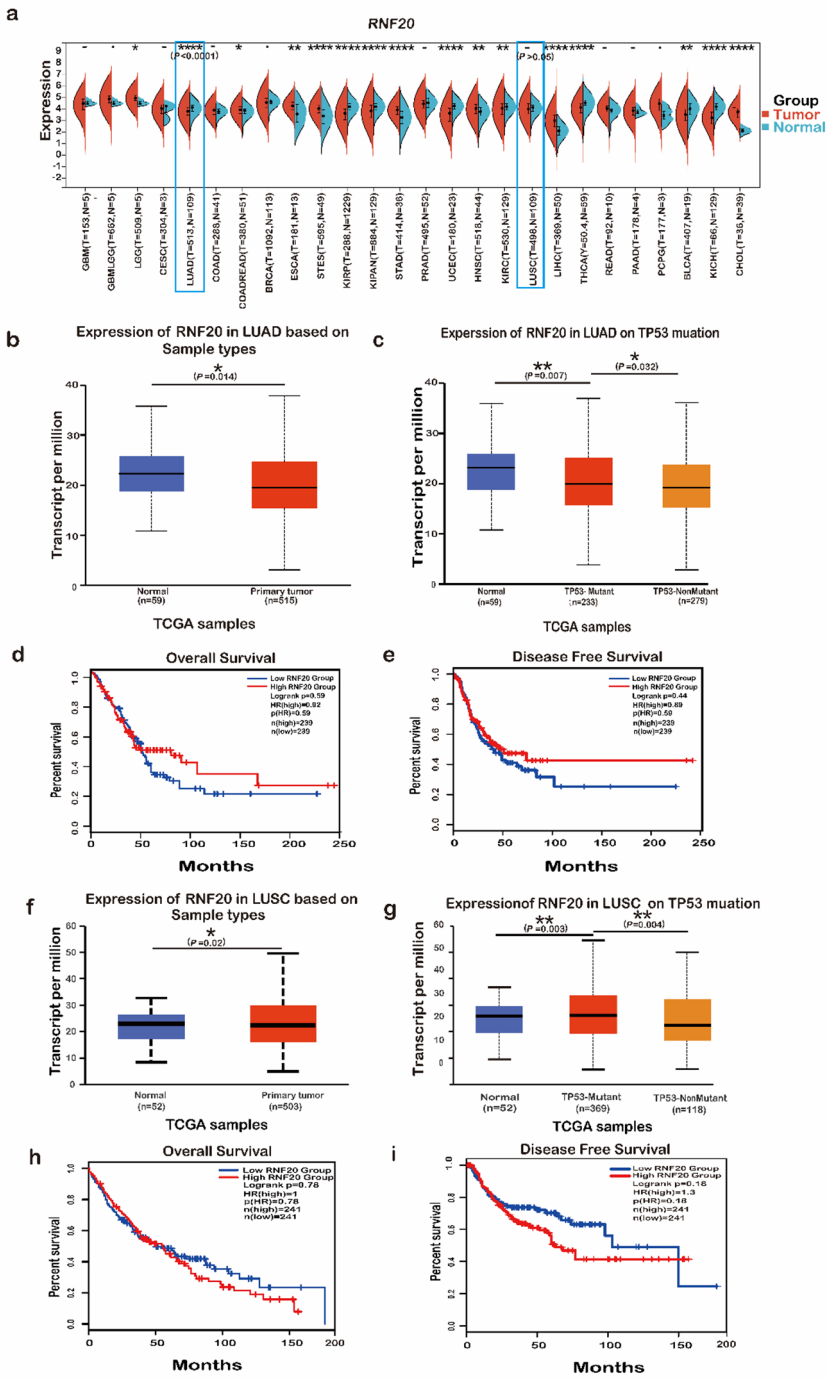


**Fig. 2**. RNF20 Expression and Clinical Features in LUAD and LUSC. (a) Expression profile of RNF20 across multiple cancers analyzed using SangerBox 3.0 based on TCGA data. (b-c) Analysis of RNF20 expression in LUAD tissues stratified by sample type and TP53 mutation status, performed using UALCAN based on TCGA data. (d-e) GEPIA survival analysis of RNF20 expression in LUAD patients using TCGA data. (f-g) Analysis of RNF20 expression in LUSC tissues stratified by sample type and TP53 mutation status, performed using UALCAN based on TCGA data. (h-i) GEPIA survival analysis of RNF20 expression in LUSC patients using TCGA data. TPM, transcripts per million; TCGA, The Cancer Genome Atlas; OS, overall survival; DFS, Disease-Free Survival. (*$P<0.05$, **$P<0.01$, ****$P<0.0001$)

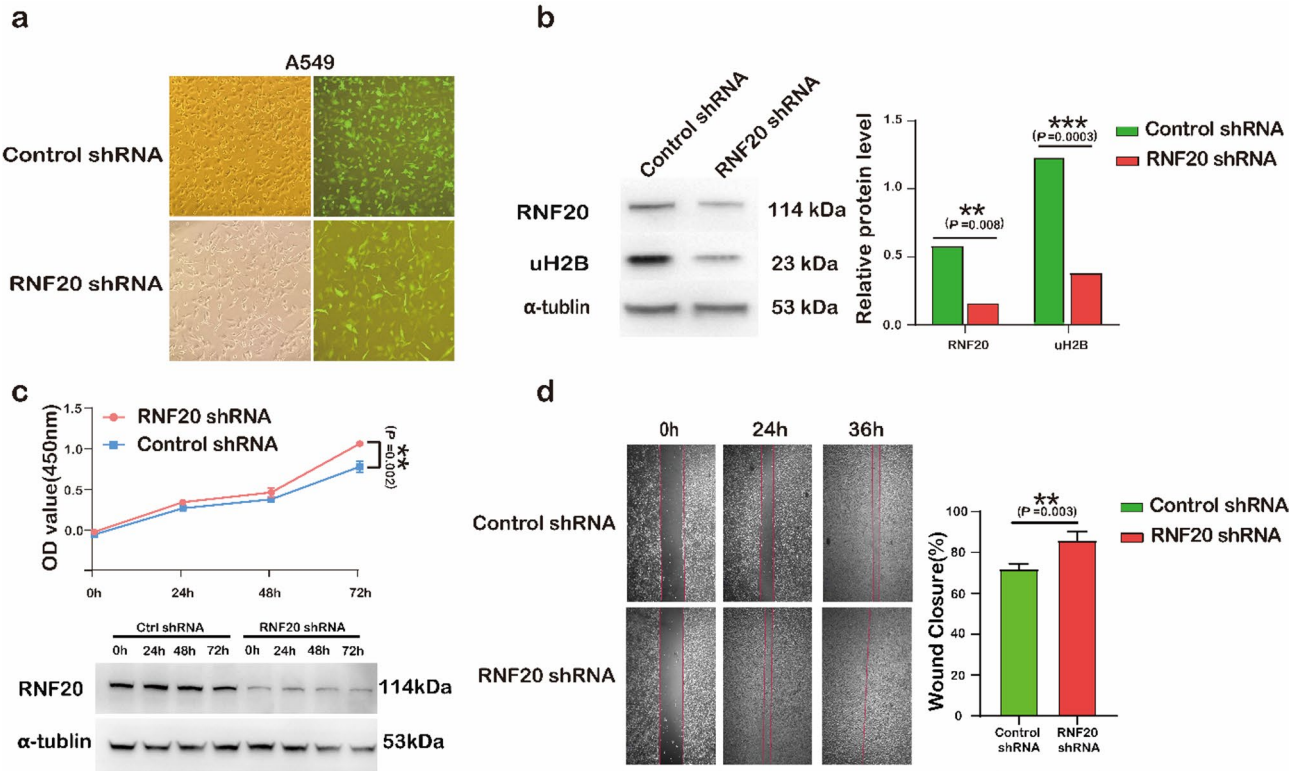


**Fig. 3**. Effects of RNF20 on A549 Cell Migration and Proliferation. (a) Transfection of A549 cells with RNF20 shRNA or control shRNA vectors. (b) Western blot analysis of RNF20 and uH2B in control and RNF20 shRNA-transfected A549 cells. (c) The CCK-8 assay analysis of cell proliferation in the RNF20-deficient group compared to controls at 24 h, 48 h, and 72 h. Western blot analysis was performed to assess time-dependent variations in RNF20 protein levels post-silencing and to validate the stable knockdown efficiency of RNF20. (d) Scratch assay showing migration in RNF20-silenced A549 cells, magnification: 4×. (**$P < 0.01$, ***$P < 0.001$)

Results showed that knockdown of RNF20 significantly promoted lung adenocarcinoma growth, aligning with findings from in vitro experiments. These findings indicate that RNF20 and its mediated H2B ubiquitination have a suppressive role in lung adenocarcinoma progression. Previous studies have shown that the Chinese gerbil is an excellent animal model for spontaneous non-obese type 2 diabetes mellitus (T2DM). This model, developed through inbreeding, demonstrates a genetic predisposition to hyperglycemia in its offspring[18,19]. The bilateral cheek pouches of Chinese hamsters exhibit unique anatomical features, including rich vascularization, easy eversion, and the absence of a complete lymphatic drainage pathway. Additionally, the density of Langerhans cells on the pouch surface is significantly reduced, and immune rejection responses are absent. These characteristics make the cheek pouches an immune-privileged site, suitable for the transplantation of foreign tissues[20]. In earlier studies, we successfully developed animal models for oral cheek pouch mucosal precancerous lesions and squamous cell carcinoma. This was achieved by applying 7, 12 – Dimethylbenz [a] anthracene (DMBA) to the mucosal surface of the hamster's cheek pouch[21,22]. The tumorigenesis in the cheek pouches of the Chinese gerbil, based on the current study, proves to be a novel approach for establishing various xenograft tumor models.

In this study, we found that knockdown of RNF20 reduced the DNA damage repair capacity of lung adenocarcinoma cells, which may be one of the mechanisms by which RNF20 affects the development of lung adenocarcinoma through H2B ubiquitination. Previous studies have shown that H2B ubiquitination plays an important role in DNA damage response[23]and our findings provide experimental evidence for this hypothesis. RNF20 downregulation was associated with defective DNA damage repair, as evidenced by increased γH2AX levels and reduced RAD51 foci in RNF20-silenced A549 cells following irradiation. These results indicate impaired homologous recombination (HR), a key pathway for double-strand break (DSB) repair. Given the critical role of HR in maintaining genomic integrity, the loss of RNF20 function likely exacerbates genomic instability, a hallmark of cancer progression[8].

Cisplatin is a widely used chemotherapy drug in clinical practice. It induces cell apoptosis by causing DNA damage, which inhibits both DNA transcription and replication[24]. PARP inhibitors induce single-strand DNA breaks, which in turn trigger double-strand breaks (DSB) during DNA synthesis[25–27]. It is widely used in the treatment and maintenance of ovarian cancer, peritoneal cancer, etc[28,29]. while studies in lung adenocarcinoma are rarely reported. In our study, chemosensitivity assays showed that RNF20-silenced A549 cells are highly sensitive to both the PARP inhibitor Olaparib and cisplatin, with significantly reduced cell viability upon treatment. This heightened sensitivity suggests that RNF20-deficient LUAD cells may exhibit synthetic lethality

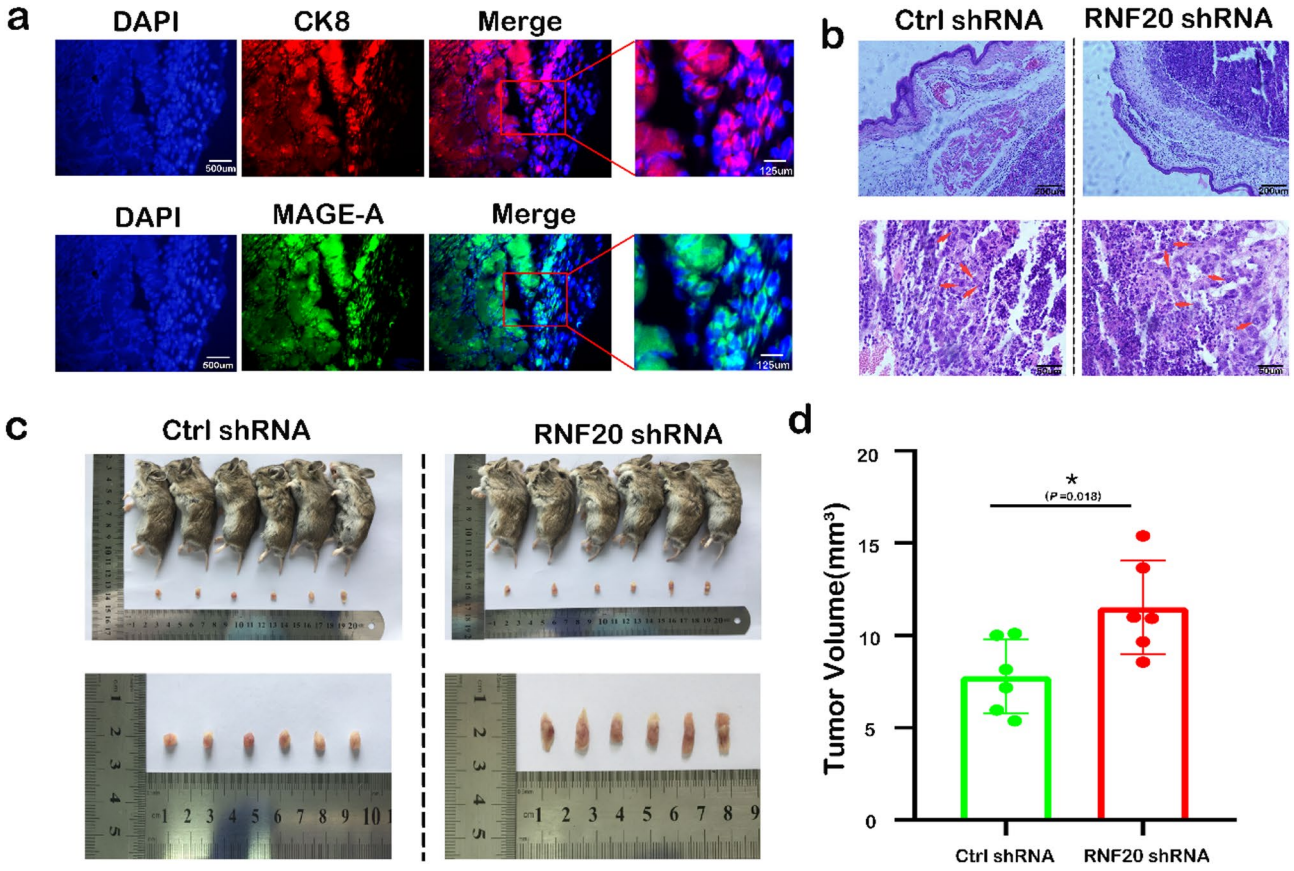


**Fig. 4**. RNF20 Knockdown Promotes Tumor Growth in a Chinese Hamster Buccal Mucosa Model. (a) Immunofluorescence staining of tumor sections for CK8 (red) and MAGE-A (green). Magnification: 40×, scale bar: 500 μm. Right panel: Magnified view of the boxed region. (b) Representative hematoxylin and eosin (H&E)-stained sections of xenograft tumors are shown. Low-magnification (Magnification: 4×, scale bar: 200 μm) and high-magnification (Magnification: 10×, scale bar: 50 μm) views demonstrate tumor cell morphology, with red arrowheads indicating regions of atypical mitotic figures and nuclear pleomorphism. (c) Representative image of tumor growth on day 3 after injection of A549 cells into the buccal mucosa. Tumor volume measured on day 3. (d)Tumors derived from RNF20-silenced cells were significantly larger, scale: mm. (*$P < 0.05$)

when treated with agents targeting DNA repair pathways. This is similar to the findings of Guppy BJ et al.[30]. More importantly, the combination of Olaparib and cisplatin demonstrated synergistic effects, with the survival rate of RNF20 shRNA-A549 cells being lower than that observed with any single drug treatment (15%). This further supports the therapeutic potential of targeting DNA repair vulnerabilities in RNF20-deficient tumors[31].

It is important to note that our study has some limitations. First, the expression of uH2B was detected using immunohistochemistry; however, this method is subject to the technical proficiency of the experimenters, introducing a degree of subjectivity in result interpretation. Second, the relatively small sample size of this study may lead to potential bias, warranting further validation in larger cohorts. Third, the study lacks both in vivo and in vitro experiments as well as deeper mechanistic investigations.

In conclusion, despite these limitations, the results of this study demonstrate that the expression of RNF20 and its mediated H2B ubiquitination is decreased in lung adenocarcinoma and closely associated with poor prognosis in lung adenocarcinoma patients. Knockdown of RNF20 promotes the proliferation, migration, and in vivo growth of lung adenocarcinoma cells, and reduces the DNA damage repair capacity of cells. These findings reveal the important role of RNF20 and H2B ubiquitination in the development of lung adenocarcinoma, providing new potential targets for the treatment of lung adenocarcinoma.

## Materials and methods

### Bioinformatics analysis

The mRNA expression level of RNF20 across various cancer types was analyzed using the SangerBox 3.0 platform (http://www.sangerbox.com/home.html). This database contains data from 60,499 tumor samples representing 26 different cancer types, integrated from The Cancer Genome Atlas (TCGA). RNF20 expression levels were compared across pan-cancer samples using the signed rank test and unpaired Wilcoxon rank-sum test. The UALCAN platform (http://ualcan.path.uab.edu/analysis-prot.html) was utilized for the analysis of RNF20

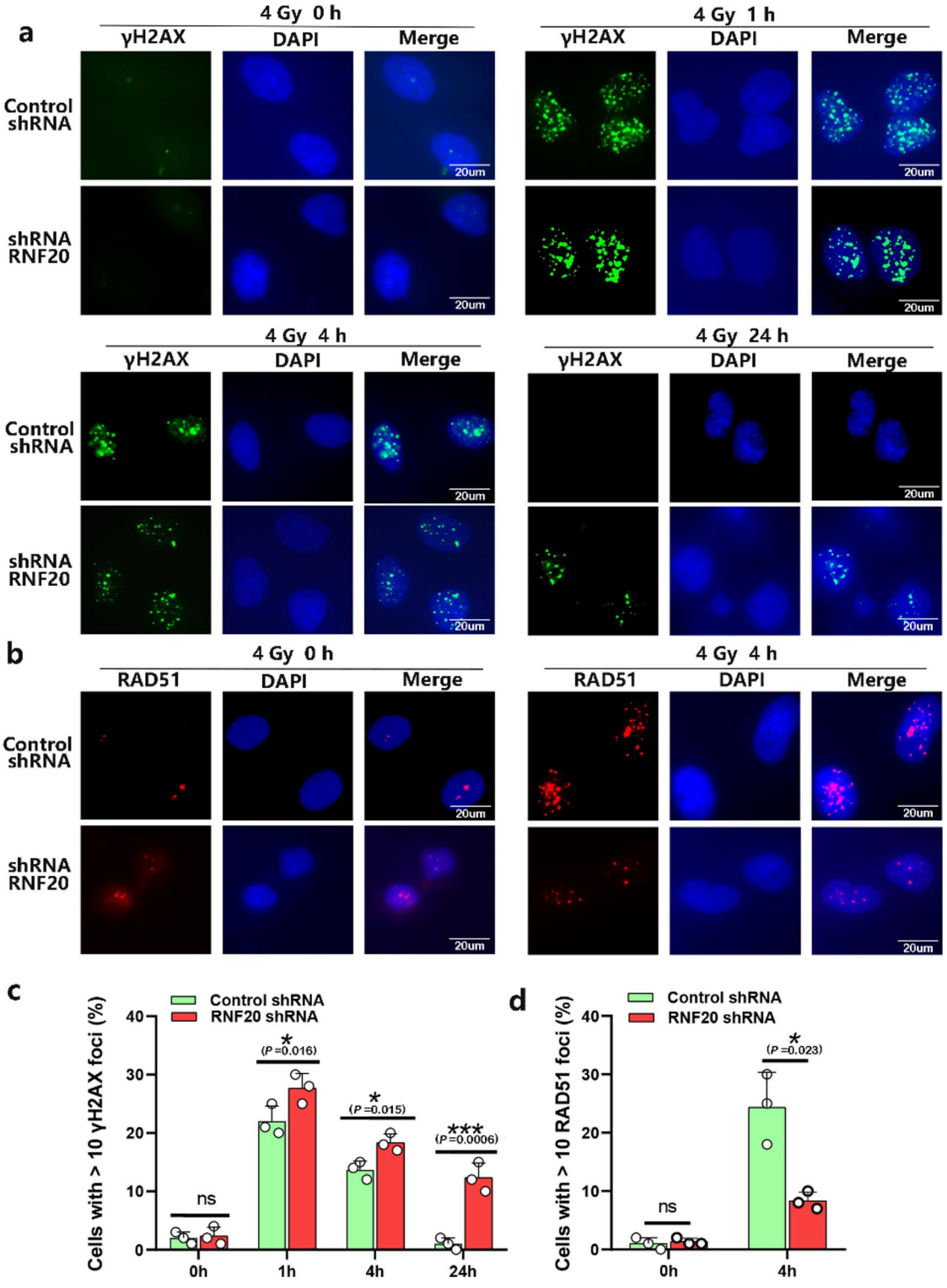


**Fig. 5**. RNF20 Knockdown Enhances DNA Damage and Impairs Double-Strand Break Repair in A549 Cells. (a-b) Representative images of γH2AX and RAD51 foci in control and RNF20-silenced A549 cells following 4 Gy irradiation, scale bar: 25 μm. Magnification: 100×, scale bar: 20 μm. (c-d) Quantification of cells with more than 5 foci. (*$P<0.05$, ***$P<0.001$)

protein expression and TP53 mutation status in LUAD/LUSC. This tool allows for the examination of gene and protein expression based on different sample types. The prognostic value of RNF20 expression in LUAD/LUSC was evaluated using the Gepia plotter tool (gepia.cancer-pku.cn), which generates survival curves to assess overall survival and Disease-free survival.

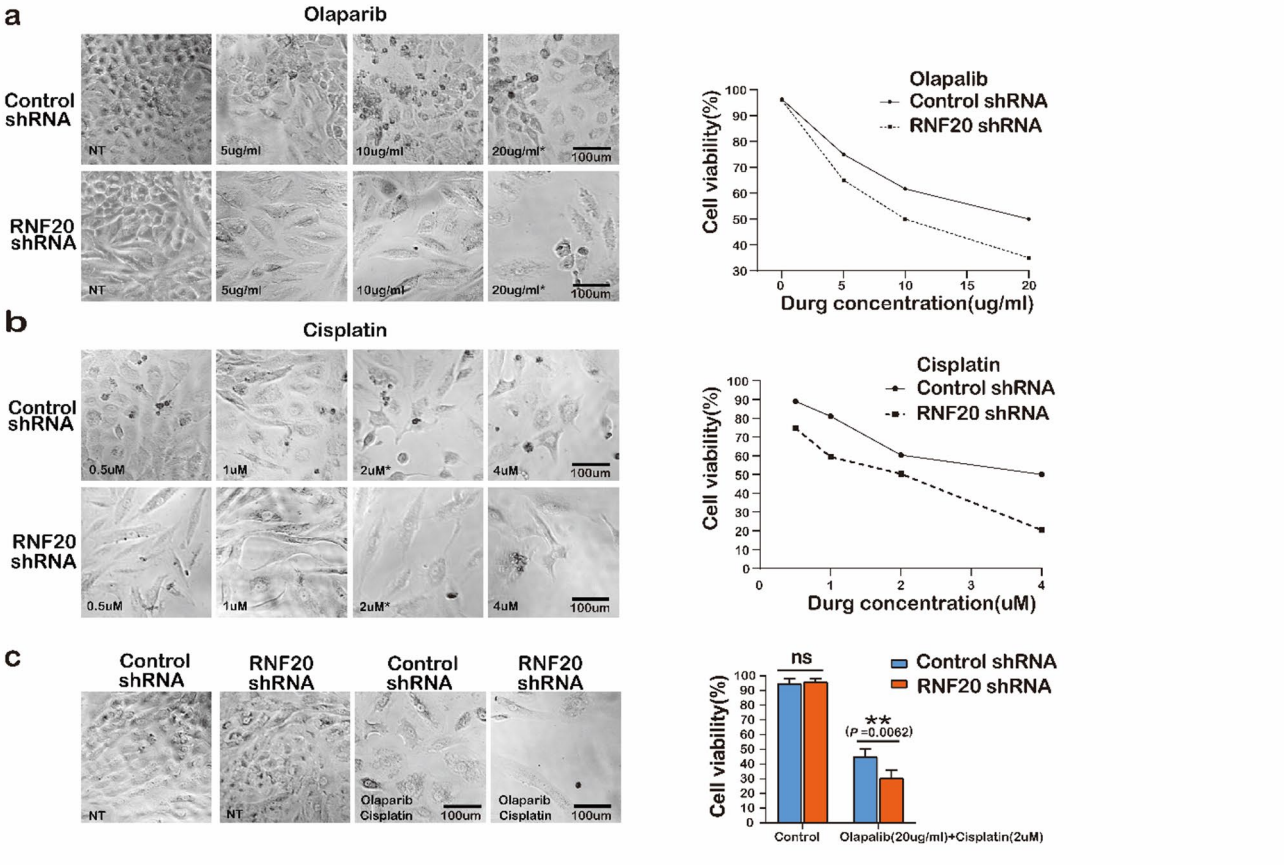


**Fig. 6**. Chemotherapy Sensitivity of RNF20-Silenced A549 Cells at Various Drug Concentrations. (a) Olaparib treatment (0, 5, 10, 20 μg/ml) decreased viability dose-dependently in Control shRNA-A549 and RNF20 shRNA-A549 cells (assessed by the trypan blue exclusion assay). RNF20 silencing conferred enhanced sensitivity at all concentrations. (b) Cisplatin treatment (0.5, 1, 2, 4 μM for 72 h) also significantly reduced viability in both groups, with a stronger effect in RNF20-silenced cells.(c) Combination treatment with Olaparib (20 μg/ml) and Cisplatin (2 μM) Data are presented as mean ± SEM, and significance was determined using a two-way ANOVA. Magnification: 10×, scale bar: 100 μm. (**$P < 0.01$)

## Antibodies and reagents

The following antibodies and reagents were used in this study for immunofluorescence (IF), immunohistochemistry (IHC), and western blot (WB): Anti-Ubiquityl-Histone H2B (Lys120) (PTM Bio, catalog number PTM-1123RM, rabbit, WB, 1:1,000), RNF20 polyclonal antibody (Proteintech, catalog number 21625-1-AP, rabbit, WB, 1:1,000), MAGE-A (6C1) (Santa Cruz Biotechnology, catalog number sc-20034, mouse, IF, 1:200), cytokeratin 8 polyclonal antibody (CK8) (Proteintech, catalog number 10384-1-AP, rabbit, IF, 1:200), γH2AX (ABclonal, catalog number AP0099, rabbit, WB, 1:500), γH2AX (Ser139) (Millipore, catalog number 05-636, mouse, IF, 1:200), RAD51 polyclonal antibody (Proteintech, catalog number 14961-1-AP, rabbit, IF, 1:200), and mouse monoclonal anti-α-tubulin (Sigma, catalog number T6074, WB, 1:50,000). Secondary antibodies included anti-mouse FITC (Sigma, catalog number F0257, ICC, 1:200), anti-mouse CY3 (BOSTER, catalog number 13L03A31, ICC, 1:50), anti-rabbit CY3 (Sigma, catalog number C2306, ICC, 1:200), and anti-rabbit HRP (Sigma, catalog number A05455, ICC, 1:2,000). Nuclear dyes included DAPI (Vector Laboratories) and. Immunohistochemistry kits, including secondary antibodies, nonspecific blockers, and DAB chromogenic agents, were purchased from Gene Technology Co., Ltd.

## Lentivirus packaging and infection

Lentiviral vectors encoding shRNA targeted human RNF20 gene (target sequence: GGGTGAACTCACGTCA GAATTCAAGAGATTCTGACGTGAGTTCAC) were purchased from ABM (Wuhan, China). A549 cells were cultured in Dulbecco's Modified Eagle Medium (DMEM; BOSTER, Wuhan, China) supplemented with 1% penicillin/streptomycin (Invitrogen) and 10% fetal bovine serum (FBS; Sigma) at 37 °C in a 5% $CO_2$ atmosphere. For RNF20 knockdown experiments, A549 cells were infected with either a lentiviral vector carrying the control shRNA (empty vector) or the RNF20-shRNA knockdown lentivirus using polybrene (5 μg/ml, Sigma) to enhance transduction efficiency. After 48 h of infection, stable cell lines were selected by 2 μg/ml puromycin (Invitrogen). The transfection procedure followed the manufacturer's instructions for lentiviral infection protocols.

### Cell proliferation assay

A total of $2 \times 10^3$ cells were seeded into each well of a 96-well plate. Cell Counting Kit-8 (CCK-8) solution (10 µl; TaKaRa, Dalian, China) was added to each well. After incubating the plate in the dark for 2 h at 37 °C, the absorbance at 450 nm was measured using a microplate reader. A blank control group was included, consisting of wells with only culture medium and CCK-8 solution, but no cells.

### Wound-healing assay

Approximately $1 \times 10^5$ cells were plated in each well of a 24-well plate and cultured until reaching a confluent monolayer. The monolayer was scratched using a sterile plastic pipette tip to create a uniform wound. The wells were then gently washed three times with phosphate-buffered saline (PBS) to remove detached cells. The remaining cells were cultured in either DMEM supplemented with 10% fetal bovine serum (FBS). Images of the wound area were captured at 0 h, 24 h, and 36 h post-scratch using a light microscope. The wound closure distance was measured using ImageJ software (https://imagej.nih.gov/ij/).

### Immunohistochemical analysis in tissue microarray (TMA) sections

For tissue microarray (TMA) analysis, sections were baked at 60 °C for 1 h, dewaxed with xylene, rehydrated in a graded ethanol series, and subjected to antigen retrieval by heating in citrate buffer (pH 6.0) under high pressure for 2 min. Endogenous peroxidase activity was blocked by soaking the sections in 3% hydrogen peroxide for 10 min. The TMA sections were incubated with the anti-uH2B primary antibody at 4 °C overnight, followed by incubation with the secondary antibody at 37 °C for 30 min. Visualization was achieved using DAB chromogen for 4–5 min, and counterstaining was performed with hematoxylin for 1 min. Sections were then differentiated in differentiation solution for 20 s, washed with tap water, dehydrated, cleared, blued, and rapidly sealed with neutral resin. After TMA chip sectioning, the slides were scanned using a pathological slide scanner (Hamamatsu, model C13210-01) equipped with the HALO digital pathology image analysis platform (Indica Labs, USA). The immunohistochemical (IHC) staining intensity of TMA samples was scored as follows: no staining (negative) = 0, light yellow (+) = 1, yellow–brown (++) = 2, brown (+++) = 3. The staining extent was scored based on the percentage of positive cells within the tissue core: no staining (negative) = 0, 1–25% = 1, 26–50% = 2, 51–75% = 3, 76–100% = 4. The final TMA score was calculated as the sum of the intensity and extent scores, with a total score ≥ 6 defined as the high uH2B expression group, and a total score < 6 defined as the low uH2B expression group.

### Immunofluorescence (IF) staining

For cell immunofluorescence (IF), A549 cells grown on glass coverslips were fixed in 4% paraformaldehyde (PFA), permeabilized with 0.3% Triton X-100 in PBS for 10 min, and then blocked with blocking solution (2% BSA, 5% goat serum, 0.5% Triton X-100 in PBS) for 40 min. Cells were incubated with the primary antibody at 37 °C for 30 min, followed by incubation with fluorescence-labeled secondary antibodies at 37 °C for 30 min. After fixation, permeabilization, and antibody incubations, the coverslips were washed three times with PBS for 5 min each. Finally, coverslips were mounted on slides using DAPI for nuclear counterstaining. The images were observed and analyzed using an Olympus fluorescence microscope (BX51). For tissue section immunofluorescence, after incubation with the anti-MAGE-A or anti-CK8 primary antibodies, the tissue sections were incubated with secondary antibodies (anti-mouse-FITC or anti-rabbit-Cy3) at 37 °C for 30 min. The sections were then stained with DAPI for nuclear visualization and rapidly sealed. Fluorescence images were captured using an Olympus fluorescence microscope (BX51). Hematoxylin and Eosin (H&E) Staining: Standard procedures were followed to perform H&E staining on paraffin-embedded tumor tissue sections. Briefly, the tissue sections were deparaffinized, rehydrated through a graded ethanol series, and stained with hematoxylin for 5–10 min. After rinsing, the sections were differentiated in acid alcohol and subsequently stained with eosin for 1–2 min. The slides were then dehydrated, cleared, and mounted using a resinous mounting medium for observation under a light microscope.

### Animals and subcutaneous lung cancer models

Male Chinese hamsters (Cricetulus griseus), aged 6–8 weeks and weighing 22–26 g, 6 mouses per group, were provided by the Experimental Animal Center of Shanxi Medical University (Production License No.: SCXK (Jin) 2019-0004). The animals were housed individually in cages within the SPF Laboratory of the Experimental Animal Center of Shanxi Medical University (Experimental License No.: SYXK (Jin) 2019-0007). The ambient temperature was maintained at 20–22 °C with a 12-hour light-dark cycle, and the animals had free access to water and maintenance pellet feed. All in vivo animal studies were approved by the Experimental Animal Welfare Ethics Review Committee of Shanxi Medical University and performed in accordance with relevant guidelines and regulations. The authors complied with the Animal Research: Reporting of In Vivo Experiments (ARRIVE) guidelines.

To induce a lung adenocarcinoma (LUAD) model, Chinese hamsters were anesthetized via intraperitoneal injection of sodium pentobarbital (30 mg/kg). Control shRNA-A549 and RNF20 shRNA-A549 cells ($2 \times 10^6$ cells suspended in 50 µl PBS per injection) were surgically implanted into the buccal mucosa of hamsters under aseptic conditions. Tumor growth was monitored daily, and lung adenocarcinoma (LUAD) xenografts were successfully established within three days post-implantation, as confirmed by macroscopic examination and caliper measurements. On day 3 post-implantation, tumor growth was assessed in anesthetized mice by blinded investigators using digital calipers to quantify tumor dimensions. Tumor volumes were calculated using the formula: Volume = 0.52 × length × width × width. At the end of the experiment, following confirmation of deep anesthesia (corneal reflex absent and no response to toe-pinch), euthanasia was humanely performed via cervical dislocation by certified personnel, adhering to the AVMA Guidelines for the Euthanasia of Animals

(2020). Subsequent tumor specimens were aseptically excised and fixed in 10% neutral-buffered formalin for 24 h prior to histopathological evaluation.

### Western blotting analysis

Total protein was extracted from tissues or cultured cells using RIPA lysis buffer (Beyotime, China) supplemented with protease and phosphatase inhibitors (Roche, USA). Protein concentrations were quantified via BCA assay (Boster USA). Equal amounts of protein (30 μg per lane) were separated by 10% SDS-PAGE and transferred onto PVDF membranes (0.22 μm, Millipore, USA). Membranes were blocked with 5% non-fat milk in Tris-buffered saline containing 0.1% Tween-20 (TBST) for 1 h at room temperature, followed by overnight incubation at 4 °C with primary antibodies: anti-uH2B、anti-RNF20 and anti-α-tublin as a loading control. After washing with TBST, membranes were incubated with HRP-conjugated secondary antibodies (1:2,000, Sigma, 1003479640) for 1.5 h at room temperature. Protein bands were visualized using ECL chemiluminescence substrate (Millipore, USA) and imaged with a GelView 6000 M (BLT, China). Densitometric analysis was performed using ImageJ software (NIH, USA), and relative protein expression levels were normalized to α-tublin. All experiments were independently repeated three times ($n = 3$).

### Drug treatment and viability measurement

A549 cells ($5 \times 10^3$) in the logarithmic growth phase were seeded into 96-well plates with three parallel wells per group and allowed to adhere overnight. After adherence, the supernatant was removed, and medium containing drugs at the indicated concentrations was added. A549 cells were treated with Olaparib (0, 5, 10 and 20 μg/ml) or cisplatin (0.5, 1, 2 and 4 μM). Cell viability was assessed by trypan blue staining after 72-hour incubation. The percentage of viable cells was calculated as: Viable cells (%) = (Viable cells / Number of viable cells) × 100.

### Statistical analysis

Data are expressed as mean ± SD and chi-square test (*$P < 0.05$, **$P < 0.01$, ***$P < 0.001$, ****$P < 0.0001$, ns, no statistical significance). SPSS 18.0 software and GraphPad Prism software were used to analyze the original data and visualization results. Kaplan–Meier analysis, log rank test and Cox regression test were used for survival analysis (Data are expressed as mean ± SEM). A value of less than 0.05 was considered statistically significant. Differences between various groups were detected using the one-way ANOVA, followed by the Dunnett's multiple-range test for multiple comparisons using GraphPad Prism 8 Software (San Diego, CA, USA).

### Source of clinical specimens and ethics

Biopsy and pathological paraffin specimens, including 162 cancerous tissues and 57 adjacent non-cancerous tissues, were collected from the pathology department of Shanxi Province Cancer Hospital between 2014 and 2021. All patients underwent surgical procedures at Shanxi Province Cancer Hospital and did not receive preoperative radiotherapy or chemotherapy. This study was approved by the Ethics Committee of Shanxi Cancer Hospital, and informed consent was obtained from all patients. The study was performed in accordance with the Declaration of Helsinki.

## Data availability

Data is provided within the manuscript.Genome expression data were sourced from the SangerBox 3.0 platform, which integrates datasets from TCGA. The UALCAN platform was employed to analyze RNF20 protein expression and TP53 mutation status in LUAD, utilizing data from TCGA. Additionally, the prognostic value of RNF20 expression in LUAD was assessed using the Gepia plotter tool (gepia.cancer-pku.cn).The more datasets used and/or analyzed during the current study are available from the corresponding author on reasonable request.

Received: 24 December 2024; Accepted: 6 June 2025
Published online: 02 July 2025

## References

1. Yin, Y. et al. Histone ubiquitination-related gene CUL4B promotes lung adenocarcinoma progression and cisplatin resistance. *Front. Genet.* **14**, 1242137. https://doi.org/10.3389/fgene.2023.1242137 (2023).
2. Siegel, R., Ma, J., Zou, Z. & Jemal, A. Cancer statistics, 2014. *CA Cancer J. Clin.* **64**, 9–29 (2014).
3. Marsh, D. J., Ma, Y. & Dickson, K. A. Histone monoubiquitination in chromatin remodelling: focus on the histone H2B interactome and Cancer. *Cancers (Basel).* **12**, 1423. https://doi.org/10.3390/cancers12113462 (2020).
4. Mishra, S., Krawic, C., Luczak, M. W. & Zhitkovich, A. Monoubiquitinated H2B, a main chromatin target of formaldehyde, is important for S-Phase checkpoint signaling and genome stability. *Mol. Carcinog.* **63**, 2414–2424. https://doi.org/10.1002/mc.23819 (2024).
5. Evangelista, F. M. et al. Transcription and mRNA export machineries SAGA and TREX-2 maintain monoubiquitinated H2B balance required for DNA repair. *J. Cell. Biol.* **217**, 3382–3397. https://doi.org/10.1083/jcb.201803074 (2018).
6. Zhou, S. et al. Role of H2B mono-ubiquitination in the initiation and progression of cancer. *Bull. Cancer.* **108**, 385–398. https://doi.org/10.1016/j.bulcan.2020.12.007 (2021).
7. Oss-Ronen, L., Sarusi, T. & Cohen, I. Histone mono-ubiquitination in transcriptional regulation and its mark on life: emerging roles in tissue development and disease. *Cells* **11**, 1456. https://doi.org/10.3390/cells11152404 (2022).
8. So, C. C., Ramachandran, S. & Martin, A. E3 ubiquitin ligases RNF20 and RNF40 are required for Double-Stranded break (DSB) repair: evidence for monoubiquitination of histone H2B lysine 120 as a novel Axis of DSB signaling and repair. *Mol. Cell. Biol.* **39** https://doi.org/10.1128/mcb.00488-18 (2019).
9. Onishi, S. et al. Structure of the human Bre1 complex bound to the nucleosome. *Nat. Commun.* **15**, 2580. https://doi.org/10.1038/s41467-024-46910-8 (2024).
10. Fanourgakis, S., Synacheri, A. C., Lavigne, M. D., Konstantopoulos, D. & Fousteri, M. Histone H2Bub dynamics in the 5' region of active genes are tightly linked to the UV-induced transcriptional response. *Comput. Struct. Biotechnol. J.* **21**, 614–629. https://doi.org/10.1016/j.csbj.2022.12.013 (2023).

11. Tarcic, O. et al. RNF20 and histone H2B ubiquitylation exert opposing effects in Basal-Like versus luminal breast cancer. *Cell. Death Differ.* **24**, 694–704. https://doi.org/10.1038/cdd.2016.126 (2017).
12. Nasim, F., Sabath, B. F. & Eapen, G. A. Lung Cancer. *Med. Clin. North. Am.* **103**, 463–473. https://doi.org/10.1016/j.mcna.2018.12.006 (2019).
13. Zhang, K. et al. Loss of H2B monoubiquitination is associated with poor-differentiation and enhanced malignancy of lung adenocarcinoma. *Int. J. Cancer.* **141**, 766–777. https://doi.org/10.1002/ijc.30769 (2017).
14. Shema, E. et al. The histone H2B-specific ubiquitin ligase RNF20/hBRE1 acts as a putative tumor suppressor through selective regulation of gene expression. *Genes Dev.* **22**, 2664–2676. https://doi.org/10.1101/gad.1703008 (2008).
15. Prenzel, T. et al. Estrogen-dependent gene transcription in human breast cancer cells relies upon proteasome-dependent monoubiquitination of histone H2B. *Cancer Res.* **71**, 5739–5753. https://doi.org/10.1158/0008-5472.Can-11-1896 (2011).
16. Chen, H. et al. KRT8 serves as a novel biomarker for LUAD and promotes metastasis and EMT via NF-κB signaling. *Front. Oncol.* **12**, 875146. https://doi.org/10.3389/fonc.2022.875146 (2022).
17. Li, Z. et al. 5-aza-2'-deoxycytidine (DAC) treatment induces the MAGE-A10 expression and improves the cytotoxicity of MAGE-A10-specific CTLs in lung cancer cells. *Transl. Cancer Res.* **9**, 1235–1245. https://doi.org/10.21037/tcr.2020.01.10 (2020).
18. Wang, L. et al. Phenotypic characterization of a novel type 2 diabetes animal model in a SHANXI MU colony of Chinese hamsters. *Endocrine* **65**, 61–72. https://doi.org/10.1007/s12020-019-01940-x (2019).
19. Shi, Z. et al. Proteomic analysis of skeletal muscle in Chinese hamsters with type 2 diabetes mellitus reveals that OPLAH downregulation affects insulin resistance and impaired glucose uptake. *Free Radic Biol. Med.* **193**, 23–33. https://doi.org/10.1016/j.freeradbiomed.2022.09.029 (2022).
20. Miedel, E. L. & Hankenson, F. C. In *Laboratory Animal Medicine* 209–245 (2015).
21. Xu, G. Q. et al. Identification and profiling of MicroRNAs expressed in oral buccal mucosa squamous cell carcinoma of Chinese hamster. *Sci. Rep.* **9**, 15616. https://doi.org/10.1038/s41598-019-52197-3 (2019).
22. Ramu, A., Kathiresan, S. & Ali Ahmed, B. Gramine inhibits angiogenesis and induces apoptosis via modulation of TGF-β signalling in 7,12 dimethylbenz[a]anthracene (DMBA) induced hamster buccal pouch carcinoma. *Phytomedicine* **33**, 69–76. https://doi.org/10.1016/j.phymed.2017.05.008 (2017).
23. Zhao, X., Wen, X. & Liu, B. Wee1 epigenetically modulates H2B mono-ubiquitination at K120 lysine and DNA double-strand break repair through phosphorylation of H2BY37-dependent manner in small-cell lung cancer. *Thorac. Cancer.* **14**, 1420–1429. https://doi.org/10.1111/1759-7714.14862 (2023).
24. Karapurkar, J. K. et al. USP28 promotes tumorigenesis and cisplatin resistance by deubiquitinating MAST1 protein in cancer cells. *Cell. Mol. Life Sci.* **81**, 145. https://doi.org/10.1007/s00018-024-05187-2 (2024).
25. Sefer, A. et al. Structural dynamics of DNA strand break sensing by PARP-1 at a single-molecule level. *Nat. Commun.* **13**, 6569. https://doi.org/10.1038/s41467-022-34148-1 (2022).
26. Kanev, P. B., Atemin, A., Stoynov, S. & Aleksandrov, R. PARP1 roles in DNA repair and DNA replication: the basi(c)s of PARP inhibitor efficacy and resistance. *Semin Oncol.* **51**, 2–18. https://doi.org/10.1053/j.seminoncol.2023.08.001 (2024).
27. Ida, N., Okura, M., Tanaka, S., Hosono, N. & Yamauchi, T. Combining inotuzumab Ozogamicin with PARP inhibitors Olaparib and Talazoparib exerts synergistic cytotoxicity in acute lymphoblastic leukemia by inhibiting DNA strand break repair. *Oncol. Rep.* **52** https://doi.org/10.3892/or.2024.8749 (2024).
28. Park, J., Cho, H. W., Lim, M. C., Choi, C. H. & Lee, J. Y. OPERA: a phase II trial of Oregovomab plus non-platinum chemotherapy in PARP inhibitor/platinum-resistant ovarian cancer. *Future Oncol.* **20**, 1893–1899. https://doi.org/10.1080/14796694.2024.2357533 (2024).
29. Jang, Y. J. et al. Therapy-related myeloid neoplasms in Korean patients with ovarian or primary peritoneal cancer treated with poly(ADP-ribose) polymerase inhibitors. *Transl Cancer Res.* **13**, 6018–6027. https://doi.org/10.21037/tcr-24-1131 (2024).
30. Guppy, B. J. & McManus, K. J. Synthetic lethal targeting of RNF20 through PARP1 Silencing and Inhibition. *Cell. Oncol. (Dordr).* **40**, 281–292. https://doi.org/10.1007/s13402-017-0323-y (2017).
31. Liu, G. et al. RPA-mediated recruitment of Bre1 couples histone H2B ubiquitination to DNA replication and repair. *Proc. Natl. Acad. Sci. U S A* **118**, 526. https://doi.org/10.1073/pnas.2017497118 (2021).


## Acknowledgements

We thank the Laboratory Animal Center of Shanxi Medical University for mouse housing and care. We also thank the Tumor Biobank of Shanxi Province Cancer Hospital for preparation of tissue slices.

## Author contributions

Laifeng Ren, Junting Jia and Guohua Song designed cellular and zoological experiments. Zhiyuan An, Ningning Yao and Wenzhong Su carried out these experiments with the assistance of Weiyang Zhang, Congqiao Zhang, Junting Yang, Qinping Guo, Pan Tian, Neng Wan, Congcong Wu. Laifeng Ren and Xiang Huang supervised the overall project and wrote the manuscript with Zhiyuan An.

## Funding

This work is supported by the Shanxi Provincial Natural Science Foundation (202403021211128, 201901D111397 and 202203021221239) and Scientific Research Foundation of Shanxi Province Cancer Hospital (SD2023003).

## Competing interests

The authors declare no competing interests.

## Ethics approval

The Ethics Research Committee of Shanxi Province Cancer Hospital approved all experiments.

## Informed consent

All clinical specimens were collected with the consent of the participants by signing an informed consent form.

## Additional information

**Supplementary Information** The online version contains supplementary material available at https://doi.org/10.1038/s41598-025-06219-y.

**Correspondence** and requests for materials should be addressed to G.S., J.J. or L.R.